

Two stage decoherence of optical phonons in long oligomers

Alexander L. Burin, Igor V. Rubtsov^{1,*}

¹*Department of Chemistry, Tulane University, New Orleans, LA 70118, USA*
(Dated: June 11, 2024)

Intramolecular energy transport is generally responsible for chemical energy balance in molecular systems. The transport is fast and efficient if energy is transferred by optical phonons in periodic oligomers, but its efficiency is limited by decoherence emerging due to anharmonic interactions with acoustic phonons. We show that in the most common case of the optical phonon band being narrower than the acoustic bands decoherence takes place in two stages. The faster stage involves optical phonon multiple forward scattering due to absorption and emission of transverse acoustic phonons, i. e. collective bending modes with a quadratic spectrum; the transport remains ballistic and the speed can be altered. The subsequent slower stage involves phonon backscattering in multiphonon processes involving two or more acoustic phonons resulting in a switch to diffusive transport. If the initially excited optical phonon possesses a relatively small group velocity, then its equilibration in the first stage is accompanied by its acceleration due to its transitions to states propagating faster. This theoretical expectation is consistent with the recent measurements of optical phonon transport in alkane chains, accelerating with increasing the chain length.

I. INTRODUCTION

Intramolecular vibrational energy transport is responsible for chemical energy balance [1–5] controlling reaction kinetics [6, 7] and it has potential applications in several fields of modern technology spanning from sustainable energy to biomedicine to thermal management [8]. It can be fast and efficient even compared to that in metals because it emerges due to covalent bonds, that are the strongest chemical bonds existing in nature [2, 9–12]. Although thermal conductivity of molecules at room temperature or below is determined substantially by low energy acoustic phonons [12–15], high energy optical phonons can be in charge for chemical energy transport. [4, 16, 17]. Indeed, typical chemical energy, exceeding phonon energy by over an order of magnitude, can be released easier to optical phonons rather than to acoustic phonons possessing considerably smaller energy. Since their propagation speeds are comparable [18], optical phonons can transfer energy more efficiently compared to the acoustic ones.

The fast and efficient energy transport by optical phonons has been demonstrated in numerous experiments [16, 19–24]. If an optical phonon is initiated within the band of a periodic oligomer chain it can propagate along the chain ballistically due to normal mode delocalization [16]. This is the most efficient energy transport realization, which is limited by decoherence and relaxation of propagating phonons induced by their anharmonic interactions with the other intramolecular vibrations and the environment [18]. Here we consider intramolecular interactions since the coupling to the environment is much weaker [5].

Following earlier work [25] we specify decoherence as optical phonon transitions holding them within the same band, while relaxation irreversibly removes optical phonons away from the band. Decoherence occurs inevitably due to interaction with low frequency acoustic phonons, while relaxation requires involvement of other optical phonons and is usually slower [25–27]. Consequently, decoherence is the first possible source of ballistic transport breakdown to consider. In the present work *we focus on optical phonon decoherence due to their anharmonic interaction with transverse acoustic phonons.*

Decoherence induced by interaction with longitudinal or torsional acoustic phonons possessing a sound like spectrum was considered in the earlier work [18]. It was shown that it is substantially suppressed in the most common situation of a forbidden Cherenkov’s like emission (or absorption), where the speed of sound c exceeds the maximum optical phonon velocity v_{max} . In this regime only relatively slow high order anharmonic processes (forth and higher) results in phonon scattering in contrast with the regime of a violated Cherenkov’s constraint $v_{max} > c$.

Decoherence due to transverse acoustic phonons representing collective bending modes needs special consideration because these phonons possess a quadratic spectrum at small wavevectors ($\omega = Aq^2$, see e. g. Ref. [28]). For this spectrum there always exist acoustic phonons with a small velocity violating the Cherenkov’s constraint, so absorption and emission are always allowed. However, if an optical phonon band is narrower than that for transverse acoustic phonons, then the absorption or emission of transverse phonon leads to a small change in the optical phonon wavevector compared to this wavevector. Consequently, absorption or emission do not modify the direction of the optical phonon propagation leading only to its forward scattering. Backscattering requires multiphonon processes occurring much slower compared to single phonon absorption or emission. Thus phonon relaxation occurs in two (fast and slow) stages. The fast stage taking around 1-10 ps involves an incomplete equilibration of the optical phonon within the states of the band with group velocities oriented towards its initial direction. At that stage the energy propagates with a nearly constant velocity similarly to the ballistic transport regime. The second stage, involving phonon backscattering, emerges after orders of magnitude longer time. Only at that stage the transport mechanism changes from the ballistic transport to the diffusive transport.

It is noticeable that if the optical phonon velocity is small in the initial state compared to a velocity typical value, then the phonon propagation speed can increase with time during the first stage. This increase can be used to interpret the observations of Ref. [29] in alkane chains, where an increase of the optical phonon transport velocity has been discovered with increasing the chain length.

In the opposite case of a narrow transverse phonon band, any absorption or emission of transverse phonons overturns the propagating phonon backwards leading to a rapid ballistic transport breakdown similarly to Ref. [18].

The paper is organized as follows. In Section II the model of optical and transverse acoustic phonons and their anharmonic interactions is introduced. In Section III the phonon decoherence is considered in terms of elementary processes of transverse phonon emission, absorption or scattering. The rates of these processes are estimated using Fermi golden rule. Our estimates are found to be consistent with the numerical simulations reported in Section IV performed using an accurate quantum mechanical [18, 30] and semiclassical [31] approaches. In Section V we examine numerically the increase of the transport speed of optical phonon with the time assuming its small initial velocity and discuss the possible connection of this result to the recent experiments in alkane chains [29]. Finally, the conclusions are formulated in Section VI.

II. MODEL

Here we introduce the model for optical phonons in a periodic chain interacting with transverse acoustic phonons. Our consideration is limited to a single optical phonon interacting with acoustic phonons, which is consistent with typical experimental conditions [16].

A. Boundary conditions and normal modes

The molecule is represented by a circular periodic chain of N identical sites (unit cells) separated by distance a . Although real chains are not circular, this model is still relevant since the propagation of phonon should not be sensitive to boundaries if the chain length $L = Na$ exceeds the coherence length of a pure ballistic propagation of phonons. In this regime the boundary conditions are not significant. In the opposite regime where the transport remains ballistic at distances exceeding molecular length the decoherence is irrelevant. The use of periodic model simplifies numerical studies because of the quasi-wavevector conservation [30] that permits us to investigate numerically longer chains than with other boundary conditions. Normal modes of the periodic chain for any specific band can be enumerated by integer numbers n and characterized by a wavevector

$$k = \frac{2\pi n}{L}, \quad L = Na, \quad n = \begin{cases} -\frac{N-1}{2}, \dots, \frac{N-1}{2}, & \text{if } N \text{ is odd,} \\ -\frac{N}{2} + 1, \dots, \frac{N}{2} & \text{if } N \text{ is even.} \end{cases} \quad (1)$$

Wavevectors are chosen to make phonon states periodic since their site dependence is determined by the exponent e^{iqan} .

B. Optical phonons

We describe the optical phonon band using a standard Hamiltonian [18]

$$\hat{H}_{\text{opt}} = \sum_k \hbar\omega_{\text{opt}}(k) \hat{a}_k^\dagger \hat{a}_k, \quad (2)$$

where the bosonic operators \hat{a}_k (\hat{a}_k^\dagger) represent annihilation (creation) operators of optical phonons characterized by the wavevector k Eq. (1) and $\omega_{\text{opt}}(k)$ stands for the wavevector dependent phonon frequency. It is a periodic function of the wavevector with the period $2\pi/a$ and it is an even function because of the time reversal invariance. We model the phonon spectrum with the simplest periodic function

$$\omega_{\text{opt}}(k) = \omega_0 + \frac{\Delta_{\text{opt}}(1 - \cos(ka))}{2}, \quad (3)$$

corresponding to the nearest neighbor interaction of site vibrations in the coordinate representation. [18] Here ω_0 is the optical phonon bandgap $0 < \Delta_{\text{opt}} \ll \omega_0$ and Δ_{opt} is the bandwidth. We consider direct bands with $\Delta_{\text{opt}} > 0$. In all calculations below we assume $\omega_0 = 1000 \text{ cm}^{-1}$ and $\Delta_{\text{opt}} = 100 \text{ cm}^{-1}$ similarly to Ref. [18], which is quite consistent with optical phonon energy band properties for organic polymer chains [32]. Generalization to a more complicated spectrum is straightforward.

The optical phonon transport is defined by the phonon current that reads

$$\hat{J} = \sum_k v_{\text{opt}}(k) \hat{a}_k^\dagger \hat{a}_k, \quad v_{\text{opt}}(k) = \frac{\partial \omega_{\text{opt}}}{\partial k} = \frac{a\Delta}{2} \sin(ka), \quad (4)$$

where $v_{\text{opt}}(k)$ is velocity of the phonon with the given wavevector k , which coincides with the group velocity for the same wavevector. This average current is evaluated numerically in Sec. IV to characterize the energy transport and its suppression by decoherence.

C. Transverse acoustic phonons

Transverse acoustic phonons, i. e. collective bending modes, are discarded in most of considerations of thermal energy transport possibly because they possess a vanishing group velocity $v(q) \propto q$ in the long wavelength limit [25],

28, 33–36], while longitudinal phonons possess a constant speed of sound. However, they provide a more significant source of dissipation as a sub Ohmic bath [28]. so they can be significant for optical phonon decoherence.

The Hamiltonian of transverse acoustic phonons for each band $\mu = 1, 2$ corresponding to two possible directions of transverse displacement can be expressed as

$$\hat{H}_{\text{tr}} = \sum_q \hbar \omega_{\text{tr}\mu}(q) \hat{b}_{q\mu}^\dagger \hat{b}_{q\mu}, \quad (5)$$

where bosonic operators $\hat{b}_{q\mu}$ ($\hat{b}_{q\mu}^\dagger$) represent annihilation (creation) operators of transverse phonons within the normal modes characterized by the operator subscript indices.

Transverse phonon frequencies are periodic functions of the wavevector, approaching 0 for $k \rightarrow 0$. We consider the simplest possible model for their spectrum, that is similar to the one for optical phonons Eq. (3) but with the zero band gap

$$\omega_{\text{tr}}^\mu(q) = \frac{\Delta_{\text{tr}\mu}(1 - \cos(qa))}{2}, \quad (6)$$

where $\Delta_{\text{tr}\mu}$ is the transverse acoustic phonon bandwidth for the specific branch μ . The spectrum in Eq. (6) is originated from a potential energy determined by local "bendings" $\epsilon_{i,\mu} = (u_{i-1,\mu} - 2u_{i,\mu} + u_{i+1,\mu})/a$ in the form $U_{\text{bend}}^\mu = \frac{A_\mu}{2} \sum_i \epsilon_{i,\mu}^2$, where the parameter A_μ is defined as $A_\mu = Ma^2 \Delta_{\text{tr}\mu}^2/4$ and M is the mass of the elementary cell.

If the molecule is immersed into a solvent, then the acoustic phonon spectrum might acquire a small gap, because the solvent violates the translational invariance [37] for atoms belonging to the molecule. Since this gap is determined by the interaction with the environment that is much weaker compared to intramolecular interaction, we ignore it.

We limit the further consideration to the interaction of optical phonons with a single transverse acoustic band, since the addition of the second band will not modify results qualitatively, while the generalization to two bands is quite straightforward. Consequently, we skip the earlier introduced index μ everywhere for the single transverse band considered below.

Similarly to Ref. [18], the relationship of acoustic and optical phonon bandwidths is a critically important parameter. We introduce it as a separate ratio parameter r defined as

$$r = \frac{\Delta_{\text{tr}}}{\Delta_{\text{opt}}}. \quad (7)$$

Acoustic bands are wider than optical bands since they are determined by direct atomic interactions through covalent bonds so usually, one has $r > 1$ (see e. g. [26]).

D. Anharmonic interaction of optical phonons with transverse phonons

Anharmonic interactions are weaker compared to harmonic ones by the ratio of the typical vibration amplitude and interatomic distance represented by the dimensionless parameter $\eta \sim 0.1$ (see Ref. [18] and Eq. (10) below). The effective strength of the k^{th} order anharmonic interaction is expressed by the parameter η^{k-2} since harmonic interaction emerges in the second order with respect to the parameter η . We consider the strongest third order anharmonic interaction similarly to Ref. [38], where it was considered for the wavepacket initiation. In the third order the only processes capable to conserve energy are determined by absorption or emission of transverse phonons by optical phonons, which can be expressed as

$$\hat{V}_{\text{anh}} = \frac{\hbar}{\sqrt{N}} \sum'_{k,q} \left[V(q, k) \hat{a}_k^\dagger \hat{a}_{k+q} \hat{b}_q^\dagger + H.C. \right], \quad (8)$$

where \sum' means that we use the periodic extension of the wavevector $k + q$ replacing it with $k + q \pm 2\pi/a$ if it is outside the domain of the wavevectors $(-\pi/a, \pi/a)$. $V(k, q)$ is the interaction constant of optical and transverse acoustic phonons; one has $V(q, k) \propto q$ for $q \rightarrow 0$ [28].

For the future consideration we take the interaction in the simplest form corresponding to the coordinate representation

$$\hat{V}_{\text{loc}} = \frac{\hbar V_0}{a} \sum_{i=1}^N \hat{a}_i^\dagger \hat{a}_i (\hat{u}_{i+1} - 2\hat{u}_i + \hat{u}_{i-1}), \quad (9)$$

where $V_0 \sim \Delta_{\text{opt, tr}}$ is the interaction constant and operators \hat{u}_i stand for the transverse displacements at the site i [18] interacting with the local density optical phonons ($\hat{a}_i^\dagger \hat{a}_i$). For this specific model the interaction constants $V(q, k)$ can be expressed as

$$V(q, k) = 2V_3 \left| \sin\left(\frac{qa}{2}\right) \right|, \quad V_3 = \eta V_0, \quad \eta = \sqrt{\frac{2\hbar}{Ma^2 \Delta_{\text{tr}}}} \sim 0.1, \quad (10)$$

This definition is used in all considerations below. The coupling constant V_3 represents a characteristic strength of anharmonic interactions that should be smaller compared to the harmonic interactions by the small factor η .

E. Full Hamiltonian

The full Hamiltonian of the system includes Hamiltonians of optical Eq. (2) and transverse Eq. (5) phonons and their interaction Eq. (8) as rewritten below for a reader convenience

$$\begin{aligned} \hat{H}_{\text{tot}} = & \sum_k \hbar \left(\omega_0 + \Delta_{\text{opt}} \frac{1 - \cos(ka)}{2} \right) \hat{a}_k^\dagger \hat{a}_k + \sum_k \hbar \Delta_{\text{tr}} \frac{1 - \cos(ka)}{2} \hat{b}_k^\dagger \hat{b}_k \\ & + \frac{2\hbar V_3}{\sqrt{N}} \sum'_{q,k} \left[\sin(qa/2) \hat{a}_k^\dagger \hat{a}_{k+q} \hat{b}_q^\dagger + H.C. \right], \end{aligned} \quad (11)$$

using Eqs. (3) and (6) for optical and transverse phonon frequencies, respectively, and Eq. (10) for anharmonic interactions.

F. Higher order anharmonic interactions

The model under consideration includes only the third order anharmonic interactions Eq. (8). However, higher order interactions are generated by the third order interactions in a perturbation theory [30]. Therefore, all decoherence channels originated from higher order interactions are present within our model Eq. (11) in the proper order in the small parameter η Eq. (10). For the future consideration we need the fourth order interaction, because it is responsible for the optical phonon backscattering in the case of a narrow optical phonon band ($r > 1$). The fourth order interaction is very important because it contains the resonant scattering of optical and acoustic phonon with opposite momentum expressed for example by the terms like $a_{-k}^\dagger b_k^\dagger a_k b_{-k}$ overturning the optical phonon current.

We derive the fourth order interaction using the celebrated Schrieffer - Wolff transformation [39] eliminating off-resonant third order anharmonic interactions to generate the resonant interaction in the fourth order. For the system Hamiltonian separated into the harmonic part \hat{H}_0 and the perturbation \hat{V} (anharmonic interactions) we introduce the unitary transformation of the Hamiltonian as $\hat{H} \rightarrow e^{\hat{S}} \hat{H} e^{-\hat{S}}$ with the anti-Hermitian operator \hat{S} defined as $[\hat{S}, \hat{H}_0] = -\hat{V}$. Then the expansion of the exponents in the power series in \hat{S} results in a disappearance of the off-resonant part of the perturbation \hat{V} (the perturbation expansion is not applicable to a resonant part) with a simultaneous generation of the fourth order interaction in the form [39]

$$\hat{H} \approx \hat{H}_0 + \hat{V}_{\text{res}} + \frac{1}{2} [\hat{S}, \hat{V}_{\text{offres}}]. \quad (12)$$

where the anharmonic interaction \hat{V} is split into resonant \hat{V}_{res} and off-resonant \hat{V}_{offres} parts.

For the specific Hamiltonian in Eq. (11) one can express the matrix \hat{S} in the form

$$\hat{S} = -\frac{1}{\sqrt{N}} \sum'_{q,k} \left[V(q, k) \frac{\hat{a}_k^\dagger \hat{a}_{k+q} \hat{b}_q^\dagger}{\omega_{\text{opt}}(k) - \omega_{\text{opt}}(k+q) - \omega_{\text{tr}}(q)} - H.C. \right]. \quad (13)$$

The modified summation \sum' means omitting resonant terms with $|\omega_{\text{opt}}(k) - \omega_{\text{opt}}(k+q) - \omega_{\text{tr}}(q)| \leq \eta^2 \Delta_{\text{opt}}$ to make both the Schrieffer-Wolff perturbation theory and the Fermi golden rule for the third order anharmonic interaction applicable, and using the proper definition of the wavevector sum $k+q$ shifted by $\pm 2\pi/a$ if necessary., to match the wavevector domain $(-\pi/a, \pi/a)$ Eq. (1).

The induced fourth order anharmonic interaction can be evaluated using Eq. (12) as

$$\widehat{V}_4 = -\frac{4\hbar V_3^2}{N\Delta_{\text{opt}}} \sum_{k,q,p} a_k^\dagger b_q^\dagger a_{k-p} b_{q+p} \left[\frac{\sin\left(\frac{q+p}{2}\right)^2 \cos\left(k - \frac{p}{2}\right)}{\left(r \sin\left(\frac{q}{2}\right) - \sin\left(k + \frac{q}{2}\right)\right) \left(r \sin\left(\frac{q}{2}\right) - \sin\left(k - p - \frac{q}{2}\right)\right)} + \frac{\sin\left(\frac{q}{2}\right)^2 \cos\left(k - \frac{p}{2}\right)}{\left(r \sin\left(\frac{q+p}{2}\right) - \sin\left(k + \frac{q-p}{2}\right)\right) \left(r \sin\left(\frac{q+p}{2}\right) - \sin\left(k - \frac{p+q}{2}\right)\right)} \right]. \quad (14)$$

In addition to the induced fourth order anharmonic interaction Eq. (12) there exists the interaction emerging similarly to the third order interaction in Eq. (8). This interaction will be also of the second order in the parameter η in Eq. (10) as that in Eq. (14), so it gives the effect comparable to that of the induced interaction. Since our consideration is qualitative and does not target the specific molecule, we can skip that interaction.

III. OPTICAL PHONON TRANSITIONS INDUCED BY ANHARMONIC INTERACTIONS

Anharmonic interactions of an optical phonon with transverse acoustic phonons Eq. (10) can lead to transitions of this optical phonon between different states emerging in the continuous spectrum for sufficiently long chains ($N \gg 1$). Such transitions affect a current associated with this phonon. Particularly, transitions accompanied by the overturn of the phonon velocity lead to ballistic transport breakdown with its further replacement with the diffusive transport.

Below we examine the phonon transitions permitted by the energy and momentum (wavevector) conservation, estimate their rates using Fermi golden rule and consider qualitatively other regimes, not handled by the Fermi golden rule. In these regimes an anharmonic interaction is either too strong to be treated as a perturbation or too weak to neglect the discreteness of the system at a finite number of sites N . All regimes are revealed in the numerical studies reported in Sec. IV.

A. Emission and absorption

1. Energy and momentum conservation

Emission or absorption of transverse phonon in a periodic chain emerges with energy and quasi-momentum (wavevector) conservation. If initially the optical phonon has a wavevector k and after emission it acquires the wavevector k' then the wavevector of emitted transverse phonon is equal to $q = k - k'$ with the accuracy to the inverse lattice period $2\pi/a$. For absorption the wavevector of absorbed phonon is given by $q = k' - k$. In either case the frequency of emitted or absorbed phonon satisfies energy conservation law in the form

$$\begin{aligned} \omega_{\text{opt}}(k) - \omega_{\text{opt}}(k') &= \omega_{\text{tr}}(k - k') \quad (\text{absorption}), \\ \omega_{\text{opt}}(k') - \omega_{\text{opt}}(k) &= \omega_{\text{tr}}(k' - k) \quad (\text{emission}). \end{aligned} \quad (15)$$

These equations are not solvable for emission or absorption of longitudinal phonons possessing the sound velocity exceeding the maximum group velocity of optical phonons in accord with the Cherenkov's emission criterion of Ref. [18]. This is not the case for the transverse phonons as illustrated in Fig. 1 for the modeling phonon spectra Eqs. (3) and (6). The solution always exists because the group velocity of transverse phonons approaches zero at small wavevector violating the Cherenkov's constraint.

Yet the graphical solutions of Eq. (15), expressing the energy conservation law, are different for different ratios r of optical and acoustic phonon bandwidths, as illustrated in Fig. 1 for $r = 1/3$ and $r = 3$. Namely, for $r < 1$ initial and final wavevector are of opposite signs, so the emission or absorption are accompanied by the overturn of the optical phonon propagation direction, i. e. backscattering, while in the opposite case $r > 1$ initial and final wavevectors are of the same signs as for scattering forward. This observation is in full accord with the analytical solution of Eq. (15) for the modeling spectra in Eqs. (3) and (6), where we got (remember, $r = \Delta_{\text{tr}}/\Delta_{\text{opt}}$)

$$\begin{aligned} q &= \frac{2}{a} \tan^{-1} \left(\frac{\sin(ka)}{r + \cos(ka)} \right) \quad (\text{emission}), \\ q &= \frac{2}{a} \tan^{-1} \left(\frac{\sin(ka)}{-r + \cos(ka)} \right) \quad (\text{absorption}). \end{aligned} \quad (16)$$

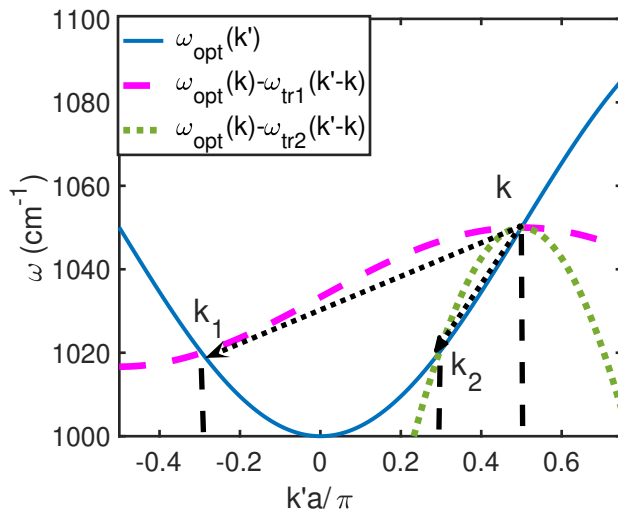


FIG. 1: Graphical solution for the emission of transverse phonon Eq. (16). Initial optical phonon wavevector is k and final is k' . Dashed (magenta) and dotted (green) lines are defined as $y(k') = \omega_{\text{opt}}(k) - \omega_{\text{tr}}(k - k')$ and used to find the solution of Eq. (15) for the emitted phonon wavevector k' as the graph intersection $y(k') = \omega_{\text{opt}}(k')$ for narrow ($\Delta_{\text{tr}} = \Delta_{\text{opt}}/3$) or wide ($\Delta_{\text{tr}} = 3\Delta_{\text{opt}}$) transverse phonon bands, respectively. Black arrows illustrate wavevector modifications after transverse phonon emission.

It is clear from both solutions Eq. (16) that the unity ratio $r = 1$ serves as the crossover regime $q = k$ for emission or $q = \pi/a - k$ for absorption, while for $r > 1$ and $k > 0$ one has $0 < q < k$ for emission and $0 < q < \pi/a - k$ for absorption leaving the wavevector k' positive. For $r < 1$ it inevitably changes direction after both absorption and emission. These conclusions remain valid for arbitrarily phonon spectra at sufficiently large ($r \gg 1$) or small ($r \ll 1$) ratios since for $r \gg 1$ the only small wavevector change leaves phonon energy within the optical band, while for $r \ll 1$ one has $q \approx 2k$ since the narrow band reflects optical phonon backwards almost statically (see also Fig. 1).

Based on this consideration we can conclude that the emission and absorption of transverse phonons occur differently depending on the ratio r of transverse acoustic and optical phonon bandwidths. If $r > 1$, then the change of the wavevector of optical phonon during the emission or absorption is smaller than the wavevector itself. Consequently, single phonon absorption or emission cannot overturn the direction of the phonon propagation. Backscattering requires higher order anharmonic processes considered below in Sec. III B. These processes can be orders of magnitude slower than a single phonon absorption or emission as it is demonstrated in the numerical simulations reported in Sec. IV. Consequently, a unidirectional propagation of vibrational energy lasts for a while. Experimentally this regime is seen quite similarly to a ballistic transport since after a phonon equilibration among the states with a certain wavevector direction the transport speed should approach a constant value given by its proper average over those states.

In the opposite regime of a smaller acoustic phonon bandwidth a single phonon absorption or emission are accompanied by the change of the direction of phonon propagation. Consequently, ballistic transport breaks down after a single or few absorption or emission events, which is consistent with our numerical studies reported in Sec. IV.

2. Absorption and emission rates

Consider the optical phonon having the wavevector k . Due to its anharmonic interaction Eq. (8) it can emit or absorb an acoustic phonon with the wavevector q Eq. (16) getting to the new state within the same band, characterized by the wavevectors $k \mp q$ due to the quasi-momentum conservation. In a first non-vanishing order in a weak anharmonic interaction the rate of this transition is given by the Fermi golden rule. According to this rule

emission and absorption rates W_{em} , W_{abs} can be expressed as (cf. Refs. [18, 40])

$$\begin{aligned}
W_{\text{em}} &= a \int_{-\pi/a}^{\pi/a} dk' V(k-k', k)^2 \\
&\times \delta(\omega_{\text{opt}}(k) - \omega_{\text{opt}}(k') - \omega_{\text{tr}}(k-k')) (1 + \nu(k-k')), \\
W_{\text{abs}} &= a \int_{-\pi/a}^{\pi/a} dk' V(k'-k, k)^2 \\
&\times \delta(\omega_{\text{opt}}(k) - \omega_{\text{opt}}(k') + \omega_{\text{tr}}(k-k')) \nu(k-k'), \quad \nu(q) = \frac{1}{e^{\frac{\hbar\omega_{\text{tr}}(q)}{k_{\text{B}}T}} - 1},
\end{aligned} \tag{17}$$

where $\nu(q)$ represents the average number of transverse phonons with the wavevector q , defined in Eq. (16).

Using the specific phonon spectra and interactions, defined by Eqs. (3), (6) and (10) we evaluate the integral in Eq. (17) as

$$\begin{aligned}
W_{\text{em}} &= 8 \frac{V_3^2}{\Delta_{\text{opt}}} (1 + \nu(q)) \frac{\sin(ka)}{r^2 + 2r \cos(ka) + 1}, \\
W_{\text{abs}} &= 8 \frac{V_3^2}{\Delta_{\text{opt}}} \nu(q) \frac{\sin(ka)}{r^2 - 2r \cos(ka) + 1},
\end{aligned} \tag{18}$$

At high temperatures where population numbers can be replaced with their classical expressions ($\nu(x) = k_{\text{B}}T/(\hbar\omega_{\text{tr}}(x))$), and $\nu(x) \gg 1$ we get

$$\begin{aligned}
W_{\text{em}} &= 8 \frac{V_3^2}{\Delta_{\text{opt}}} \frac{k_{\text{B}}T}{\hbar\Delta_{\text{tr}} \sin(ka)}, \quad W_{\text{abs}} = 8 \frac{V_3^2}{\Delta_{\text{opt}}} \frac{k_{\text{B}}T}{\hbar\Delta_{\text{tr}} \sin(ka)}, \\
W_{\text{tot}} &= W_{\text{abs}} + W_{\text{em}} = 16 \frac{V_3^2}{\Delta_{\text{opt}}} \frac{k_{\text{B}}T}{\hbar\Delta_{\text{tr}} \sin(ka)},
\end{aligned} \tag{19}$$

where W_{tot} represents the total decay rate of the optical phonon.

The lifetime T_{rel} of the optical phonon in the given quantum state can be estimated as the inverse total decay rate

$$T_{\text{rel}} = \frac{1}{W_{\text{tot}}}. \tag{20}$$

The inverse lifetime defines the inelastic width of the energy level as \hbar/T_{rel} .

B. Backscattering for a large bandwidth ratio $r > 1$

1. Backscattering at high temperature. Fourth order processes.

At a large bandwidth ratio $r > 1$ backscattering can be originated from the phonon scattering expressed by the fourth order anharmonic interaction Eq. (14), which is the next anharmonic correction to the third order interaction considered above. There is no constraints for the energy conservation for phonon scattering as can be illustrated for instance by the resonant backscattering of optical and acoustic phonons with opposite wavevectors resulting in their wavevector exchange. Such processes require the presence of excited acoustic phonons that is possible if the thermal energy $k_{\text{B}}T$ is at least comparable or larger than the transverse bandwidth $\hbar\Delta_{\text{tr}}$. In the opposite case of low temperature $k_{\text{B}}T \ll \hbar\Delta_{\text{tr}}$ multiphonon emission is needed for the optical phonon back scattering as shown below in Sec. III B 2.

The back scattering rate can be estimated using Fermi golden rule with the interaction in Eq. (12) as a perturbation. Because of the large number of scattering outcomes we do not attempt to calculate a specific relaxation rate, but instead consider its dependence on the anharmonic coupling V_3 , bandwidth ratio r assuming $r > 1$ and temperature T in a thermodynamic limit of a sufficiently long chain, where the continuum approach is applicable (see discussion of discreteness in Sec. III C 2).

At high temperatures $k_{\text{B}}T > \hbar\Delta_{\text{tr}}$ one can estimate the coupling matrix element for the processes relevant for the optical phonon overturn in Eq. (12) as $\hbar V_4 = \hbar V_3^2 k_{\text{B}}T / (r^3 \Delta_{\text{opt}}^2)$. The transition rate produced by the Fermi golden rule can be then estimated as

$$W_4 \sim \frac{V_4^2}{\Delta_{\text{tr}}} = C \frac{V_3^4 (k_{\text{B}}T/\hbar)^2}{r^7 \Delta_{\text{opt}}^5}, \quad C \approx 3 \cdot 10^4, \tag{21}$$

where C is the dimensionless proportionality constant determined numerically below in Sec. IV B 4. Eq. (21) is approximately consistent with the numerical results for the phonon current relaxation rate reported below in Sec. IV, where the large absolute value of the proportionality constant C in Eq. (21) is explained on a semiquantitative level. The fourth order anharmonic interaction with longitudinal phonons should result in a relaxation rate behaving similar to Eq. (21) since longitudinal and transverse branches are weakly distinguishable for a large phonon wavevectors $k, q \sim \pi/a$ relevant for that regime.

2. Backscattering at low temperature: multi-phonon emission

If the temperature is very low so there are no acoustic phonons capable of scattering initially excited optical phonon backwards, then the only remaining option for the optical phonon overturn is a multi-phonon emission. Such process is forbidden for longitudinal acoustic phonons possessing the velocity exceeding that of optical phonons [18], but it is allowed for transverse acoustic phonons even for $r \gg 1$ as shown below.

As an illustration consider the overturn of the optical phonon with the wavevector k by means of the emission of n transverse phonons with wavevectors q_1, q_2, \dots, q_n and total wavevector $\sum_{i=1}^n q_i = k$, which is the minimum wavevector change corresponding to the overturn that should take place simultaneously with the frequency change $\sum_{i=1}^n \omega_{\text{tr}}(q_i) = (\omega_{\text{opt}}(q) - \omega_{\text{opt}}(0))$ due to energy conservation law. The most efficient emission takes place at the minimum number n of emitted transverse phonons since the emission rate decreases exponentially as η^{2n} with increasing n (see Eq. (10) for the definition of η).

It can be shown rigorously for our specific phonon spectrum Eq. (6) and generalized to any monotonic function $\omega_{\text{tr}}(q)$ that the optimum emission regime is realized for all identical emitted transverse phonons with wavevectors $q_i = k/n$. Assuming a large number of phonons $n \gg 1$, which is valid for $r \gg 1$ we can approximate the total emitted energy as $\hbar \Delta_{\text{tr}} a^2 k^2 / (4n)$ and we estimate the minimum number of emitted phonons needed for the overturn as

$$n = \eta_{\text{ph}} r, \quad \eta_{\text{ph}} = \frac{k^2 a^2}{4 \sin(ka/2)^2}. \quad (22)$$

Thus, in our model the number of transverse phonons needed to be emitted is proportional to the bandwidth ratio r with the proportionality coefficient η_{ph} ranging from 1 to $\pi^2/4 \approx 2.5$. The multiphonon emission rate W_{mult} is proportional to the squared coupling constant for the n phonon process. Consequently, we expect that

$$W_{\text{mult}} \propto \eta^{2\eta_{\text{ph}} r}, \quad (23)$$

where $\eta \sim 0.1$ Eq. (10). Additional dependence on the number of emitted phonons can be originated from the wavevector dependence of the n -phonon interaction constant. We do not investigate this dependence in detail, because we were not able to reproduce this regime numerically as reported in Sec. IV A, so it cannot be compared to any experimental or numerical observation.

C. Regimes of Fermi golden rule failure

Here we consider the regimes that cannot be characterized by Fermi golden rule rates. These considerations are needed for understanding dynamics observed in numerical simulations reported below in Sec. IV for very large or very small anharmonic interactions.

The Fermi golden rule fails at very large anharmonic interactions V_3 in Eq. (10), where the perturbation theory is no more applicable, and at very small anharmonic interactions, where the discreteness of the phonon spectrum becomes important. Below we address both regimes.

1. Strong anharmonic coupling

Consider the evolution of the initial harmonic state a with certain wavevectors of all phonons. The population $P_a(t)$ of this state decreases with time due to anharmonic interactions. At short times it decreases as $P_a(t) = 1 - W_*^2 t^2$, where $W_* = V_*/\hbar$ and $V_* = \sqrt{\sum_{b \neq a} V_{ab}^2}$, where V_{ab} is the off-diagonal matrix element of anharmonic interaction coupling harmonic states a with any other harmonic state b possessing harmonic energies E_a and E_b , respectively. For a weak anharmonic interaction, where Fermi golden rule is applicable, this decay slows down at times much shorter than the effective minimum relaxation time $T_* \approx 1/W_*$, since the squared time dependence for each specific

state b saturates at time $t \sim \hbar/|E_a - E_b|$. For a strong interaction the maximum rate W_* gives a reasonable estimate for the relaxation rate consistent with the numerical results of Sec. IV.

For the future comparisons with numerical results we report below the maximum relaxation rate W_* and its asymptotic behaviors at high and low temperatures evaluated for the anharmonic interaction Eq. (10) as

$$W_* = \sqrt{\frac{1}{N} \sum_q 4V_3^2 \sin^2(qa/2) \left(1 + \frac{2}{e^{\frac{\hbar\omega_{\text{tr}}(q)}{k_{\text{B}}T}} - 1}\right)} = \begin{cases} \sqrt{2}V_3, & k_{\text{B}}T \ll \Delta_{\text{tr}} \\ 4\sqrt{2}V_3 \sqrt{\frac{k_{\text{B}}T}{\Delta_{\text{tr}}}}, & k_{\text{B}}T \gg \Delta_{\text{tr}}. \end{cases} \quad (24)$$

2. Weak anharmonic coupling: effect of discreteness

The Fermi's golden rule is applicable to the continuous spectrum in the infinite chain limit. The spectrum can be treated as continuous if the energy uncertainty associated with the specific state decay rate Eq. (18) defined as $\hbar W_{\text{tot}}$ exceeds the interlevel splitting given by $\Delta E \approx (2\pi\hbar/L) \max(|\partial\omega_{\text{tr}}(k)/\partial k|, |d\omega_{\text{opt}}(k)/dk|)$, where L is the chain length. Comparing two energies to each other we come up with the constraint on the strength of anharmonic interaction V_3 needed for the Fermi's golden rule to be applicable, that can be expressed as

$$V_3 > \max(1, \sqrt{r}) \frac{\Delta_{\text{opt}}}{\sqrt{N}} \begin{cases} \sqrt{\frac{\pi(1+2r \cos(ka)+r^2)}{8}}, & k_{\text{B}}T \ll \hbar\Delta_{\text{tr}} \\ \frac{\sin(ka)}{4} \sqrt{\frac{\pi r \hbar \Delta_{\text{opt}}}{k_{\text{B}}T}}, & k_{\text{B}}T \gg \hbar\Delta_{\text{tr}}. \end{cases} \quad (25)$$

What to expect if Eq. (25) is not satisfied and the discreteness is significant? At low temperature and reasonably short chains $N \sim 10$ the non-ergodic behavior can emerge [5, 30, 41, 42] similarly to that found in the earlier work [18], where the interaction of optical phonons with longitudinal acoustic phonons was considered. In the non-ergodic or many-body localized regime [5, 30] optical phonon current in a periodic chain will never relax to zero staying close to its initial value, except for the states with the total wavevector 0 or π/a where it disappears in average due to the inversion symmetry. Yet in the non-ergodic regime the current does not relax to zero but coherently oscillates switching between positive and negative values.

There is a greater chance to observe the localized regime for larger bandwidth ratio r since the critical strength of anharmonic coupling separating discrete and quasi-continuous regimes grows with r as $r^{3/2}$. At high temperature the ergodic behavior should be restored due to phonon scattering. All these expectations are reasonably consistent with the results of numerical simulations reported in Sec. IV.

IV. NUMERICAL STUDIES

The present section targets verification of the analytical expectations of Sec. III using as accurate as possible numerical modeling of the optical phonon transport. We study how the transport in periodic atomic chains is affected by interaction with transverse acoustic phonons using fully quantum mechanical or semi-classical approaches for periodic atomic chains. The quantum mechanical treatment reported in Sec. IV A is developed similarly to the earlier work [18] considering longitudinal acoustic phonons. It is limited to relatively short chains and small total energies (very low temperatures) because of the exponential increase of the number of significant quantum states with energy and number of sites N , which prohibits an accurate numerical diagonalization for longer chains.

The second approach (Sec. IV B) treats acoustic phonons and their interaction with the optical phonon classically, which permits us to characterize large systems at high temperatures, where this consideration is reasonably justified.

A. Quantum mechanical treatment

The full quantum-mechanical treatment of optical phonon transport is quite similar to the earlier work [18] (see also Ref. [30]). Exact diagonalization of the system Hamiltonian Eq. (11) is not possible since the basis of its possible states is infinitely large. However, for the states with relatively small energies we can limit our consideration to a number of acoustic phonons not exceeding a certain maximum number n_{max} and perform the full diagonalization with that limited basis [18, 30]. Our approximation can be validated considering the dependence of certain parameters of interest on the number n_{max} . In most of the calculations we investigated the time evolution of the probability $P_n(t)$ to find the excited optical phonon in its initial state with a certain wavevector $k = 2\pi n/L$ and we used its infinite time limit $P_n(\infty)$ as a convergence control parameter.

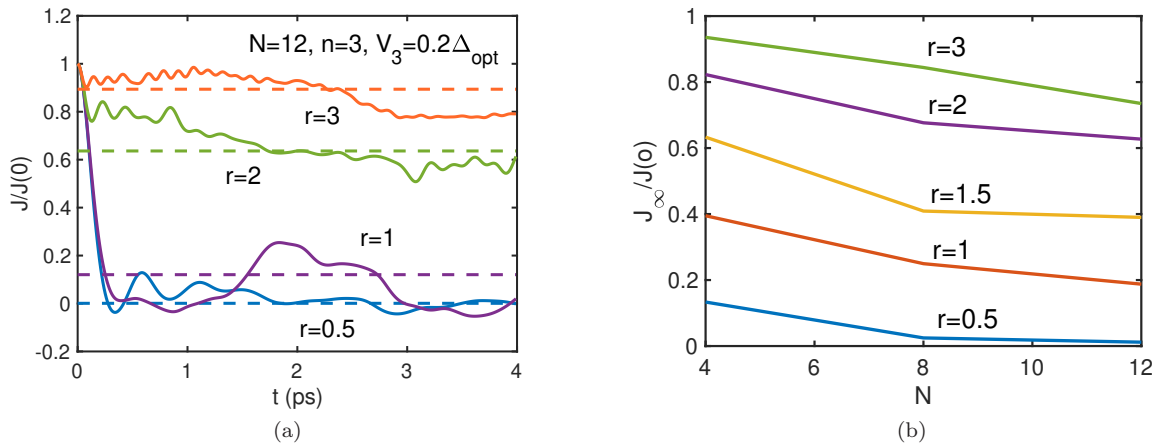


FIG. 2: Time dependence of currents (a) and size dependence of time averaged currents J_∞ (b) for different ratios r of transverse acoustic and optical bandwidths.

The calculations reported below are performed for a periodic chain of $N = 12$ sites and the anharmonic interaction strength $V_3 \leq 0.5\Delta_{\text{opt}}$. In this specific case a good convergence for probabilities $P_n(\infty)$ is obtained for $n_{\text{max}} = 6$, which corresponds to the basis of 12376 states. The difference of the results for $n_{\text{max}} = 5$ and $n_{\text{max}} = 6$ is always less than few percents and their difference for $n_{\text{max}} = 6$ and $n_{\text{max}} = 7$ is less than 1%. Therefore, we believe that our method gives a good approach to the actual quantum evolution of the system.

We investigate the relaxation of the current for the initially excited optical phonon with the wavevector $k = 2\pi n/(aN)$. The state with $n = N/4 = 3$ is chosen because it is located in the middle of the band and possesses a maximum phonon velocity $v(k) = \Delta_{\text{opt}} \sin(ka)/2$ realized at $ka = \pi/2$ Eq. (4). The results for other initial wavevectors are quite similar, except for $n = 0$ where non-ergodic behavior was seen for $V < 0.5\Delta_{\text{opt}}$ for any considered bandwidth ratios because it is the lowest energy optical phonon state having no decay channels. Since the observed dependence on the initial wavevector is quite similar to that reported in Ref. [18] we do not show the results of calculations for $n \neq 3$.

We investigated two different initial states including (A) the initial state with a single excited optical phonon with the wavevector $k = 2\pi n/L$ and (B) the two-phonon initial state with a single excited optical phonon with the same wavevector k and a single acoustic phonon with the wavevector $-k$. The case (A) earlier used in Ref. [18] is targeted to examine the relaxation due to the emission of acoustic phonons, while in the case (B) we also investigate the effect of resonant backscattering on the optical phonon current for a large bandwidth ratio $r > 1$. The more complicated initial conditions are briefly discussed in the end of the present section.

1. Single excited optical phonon

The time evolution of the optical phonon current for the initial state containing only one excited optical phonon with the wavevector $k = \pi/(2a)$ ($N = 12$) is shown in Fig. 2.a for four different bandwidth ratios r . We choose the maximum coupling strength $V_3 = 0.2\Delta_{\text{opt}}$, where the perturbation theory with respect to anharmonic interaction is still applicable. Infinite time limits of current shown by dashed lines are evaluated averaging current over time, that sets all oscillating contributions to zero as in Refs. [18, 43].

The observed evolution of currents for bandwidth $r \leq 1$ and $r > 1$ are clearly different. For $r \leq 1$ the current rapidly decreases to the small value compared to the initial current $I(0)$, while for $r = 2$ and 3 it changes weakly compared to its initial value. We interpret this difference as the separation between ergodic ($r = 0.5$ and 1) and non-ergodic ($r = 1.5, 2$ and 3) regimes. In an ergodic regime the time averaged current represented by its infinite time limit should approach its thermodynamic average of 0 in the thermodynamic limit of an infinite system $N \rightarrow \infty$.

We evaluated the size (N) dependence of a time-averaged current J_∞ corresponding to its infinite time limit as reported in Fig. 2.b. The size dependence, indeed, shows fast reduction of J_∞ with the system size for $r \leq 1$ and a substantially weaker size dependence for $r > 1$ that is consistent with our assumption of the transition between ergodic and non-ergodic behaviors at $r \approx 1$. However, we expect that at larger sizes N ergodic behavior should be restored for an arbitrary r due to forward scattering and higher order anharmonic interactions. This contrasts to the case of optical phonon interaction with longitudinal phonons where any transitions for a single excited optical phonon

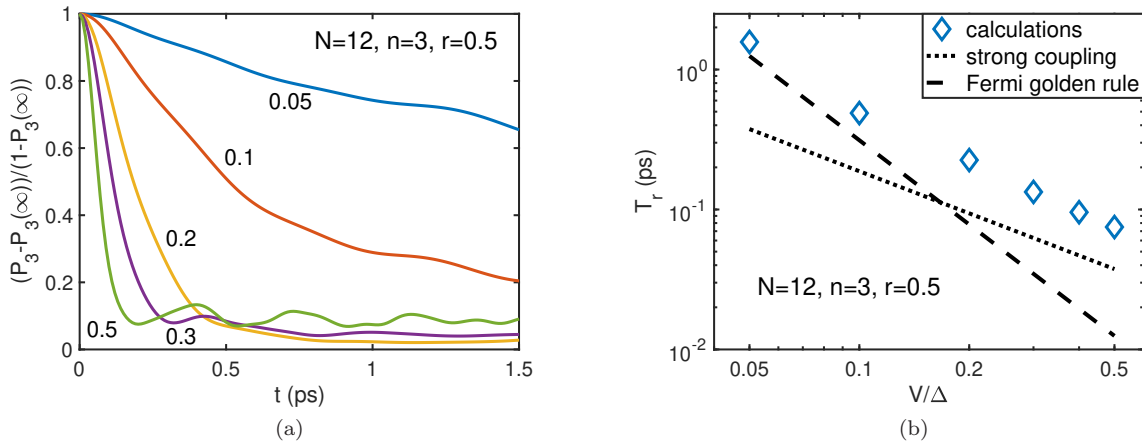


FIG. 3: (a) Relaxation of the population of the optical phonon midband state $n = 3$ for 12 site chain, and bandwidth ratio $r = 0.5$ at different strengths of anharmonic interaction. (b) Dependence of population relaxation time on the strength of anharmonic interaction shown together with the rate predicted by the Fermi's golden rule (18) shown by the dashed line and characteristic minimum lifetime $1/W_*$ Eq. (24) shown by the dotted line.

are forbidden in the regime of Cherenkov's constraint [18].

We investigated the relaxation of the population of the initially excited state $P_n(t)$ in the ergodic regime $r = 1/2$ to compare relaxation times estimated using Fermi's golden rule (inverse relaxation rate W_{tot} Eq. (18)) with their numerical estimates. The numerical relaxation time T_{rel} is defined using time dependent populations $P(t)$ shown in Fig. 3.a setting $P(T_{\text{rel}}) = P_\infty + (1 - P_\infty)e^{-1}$ for $n = 3$. Numerical relaxation times are shown by diamonds in Fig. 3.b vs. anharmonic coupling strengths and compared to the Fermi's golden rule estimate W_{tot}^{-1} (Eq. (18), dashed line) and the minimum relaxation time W_*^{-1} realized for a strong anharmonic coupling (Eq. (24), dotted line). It turns out that relaxation time switches between two regimes with increasing the coupling strength V_3 as expected. For $V_3 < 0.03\Delta_{\text{opt}}$ the relaxation is no more seen, but instead the current oscillates around its average value close to its initial value. This suggests an ergodicity breakdown emerging at $V_3 < 0.03\Delta_{\text{opt}}$ with the current evolution similar to observed behaviors for $r \geq 2$ as shown in Fig. 2. a.

Non-ergodic behaviors are caused by discreteness as discussed in Sec. III C 2. An increase of the number of sites N should most probably eliminate that behavior even for $r > 1$ in a thermodynamic limit of $N \rightarrow \infty$ due to allowed forward scattering that was lacking in the previous study [18].

2. Two phonon initial state

To investigate the effect of a resonant two-phonon interaction onto the system dynamics we modified the initial conditions compared to Sec. IV A 1 using an optical phonon with the wavevector $k = 2\pi n/L$ ($n = 3, N = 12$) and one transverse acoustic phonon with the opposite wavevector $-k$. We focus only on a nonergodic regime $r > 1$ since in the ergodic regime the current evolution is practically the same as for the initial conditions of a single excited optical phonon reported in Sec. IV A 1.

For two-phonon initial condition the time-averaged optical phonon current approaches zero because of the inversion symmetry of the problem for a total wavevector equal 0 suggesting that each eigenstate of the problem is composed by the symmetric or antisymmetric combination of pairs of states with all opposite wavevector like $|k, -k\rangle$ and $| -k, k\rangle$ for two-phonon state. The initial state used in Sec. IV A 1 possesses a wavevector $k = \pi/(2a)$. The conservation of the wavevector does not allow a system transition to the symmetric state with the opposite wavevector, since the difference of two state wavevectors π/a is not equal to an integer number of inverse lattice periods $2\pi/a$. Consequently, the inversion symmetry is broken and the average current differs from zero.

For two phonon initial condition and $r \geq 2$ the current shows nearly coherent oscillations around zero, as illustrated in Fig. 4.a (grey line) for a bandwidth ratio $r = 4$, in a stark contrast with the time evolution for a single phonon initial condition, as shown in the same graph (magenta line). Similar oscillations were found for a wide range of anharmonic coupling strengths and bandwidth ratios $r \geq 2$.

To interpret the observed coherent oscillations we employ the secular perturbation theory limiting our consideration to the only two resonant states $|k, -k\rangle$ (the initial state) and $| -k, k\rangle$ (the symmetric state) possessing identical

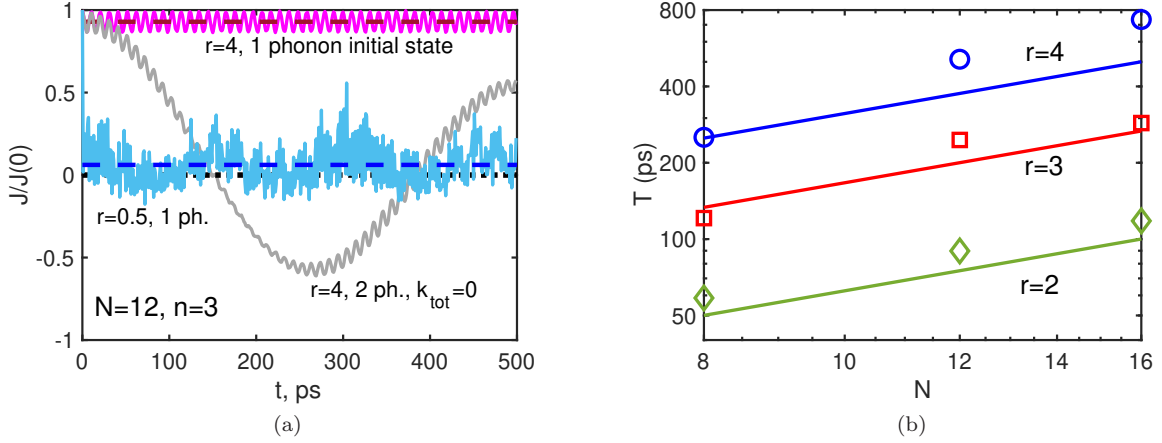


FIG. 4: Coherent oscillation of current for a two phonon initial state with the total wavevector 0. (a) Dependence of current on time. (b) Dependence of oscillation period on chain length at different ratios of bandwidths r . Straight lines show the expected oscillation period due to resonant interactions in Eq. (26). Anharmonic coupling strength is $V_3 = 0.2\Delta_{\text{opt}}$.

harmonic energies and coupled by the fourth order anharmonic interaction $V(k, -k, -k, k) = 16\hbar V_3^2 / (N\Delta_{\text{opt}}(r^2 - 1))$ Eq. (14). For the given initial condition the system coherently oscillates between these two states possessing opposite optical phonon currents with the period

$$T_{\text{res}} = \frac{2\pi\hbar}{V(k, -k, -k, k)} = \frac{2\pi(r^2 - 1)N\Delta_{\text{opt}}}{16V_3^2}. \quad (26)$$

In Fig. 4.b we show the dependence of numerically estimated oscillation periods (symbols) on a system size and bandwidth ratios. Here we used the maximum number of acoustic phonons equal to 5 which is justified for $N \leq 12$ but questionable for $N = 16$. Numerical estimates are consistent with the theory predictions Eq. (26) shown by the straight lines. Coherent oscillations of current suggest a non-ergodic behavior in spite of average current vanishing.

We also examined more complicated initial conditions. If one use three phonons including one optical phonon, one acoustic phonon with an opposite wavevector and one additional acoustic phonon, the time averaged current approaches an intermediate value between 0 and its initial value $J(0)$ (for instance, if we add one more transverse acoustic phonon with the same wavevector $-k$ we got $J_{\infty} \approx J(0)/2$) in the limit of small anharmonic coupling. This is a typical behavior for a non-ergodic regime. In the ergodic regime realized for long chains $N \gg 1$ and/or high temperatures $k_B T \gg \hbar\Delta_{\text{opt}}$ the fourth order anharmonic interaction Eq. (14) leads to the relaxation investigated below in Sec. IV B using the semiclassical approach.

B. Semiclassical treatment

1. Semiclassical Model

Since most of experiments are performed at room temperature the assumption of a low temperature made in the previous section is not satisfied there. At room temperature a typical thermal energy $k_B T$ is comparable to the acoustic phonon bandwidth and exceeds the optical phonon bandwidth. Under those conditions

$$\Delta_{\text{opt}}, \Delta_{\text{tr}} < k_B T \quad (27)$$

we employ a semiclassical treatment of acoustic phonons to simplify the consideration. Here we use it in the form of Refs. [31] developed to investigate charge transfer in DNA.

The semiclassical approach can be formulated as follows. We describe the optical phonon by the wavefunction within the momentum (wavevector) representation

$$|\psi\rangle = \sum_k c_k |k\rangle, \quad (28)$$

where symbols $|k\rangle$ stands for the state with the given wavevector k and coefficients c_k are wavefunction amplitudes determining probabilities $P_k = |c_k|^2$ to find the phonon in the state with the given wavevector k , which are subject to the normalization condition $\sum_k P_k = 1$. Transverse phonons are characterized by classical coordinates u_q and momenta p_q also defined in the wavevector representation.

The system is described by the classical Hamiltonian Eq. (11)

$$H = \sum_q \frac{p_q p_{-q}}{2M} + \frac{M}{2} \sum_q \omega_{\text{tr}}(q)^2 u_q u_{-q} + \sum_k \hbar \omega_{\text{opt}}(k) c_k^* c_k + 2V_3 \sqrt{2\hbar M \Delta_{\text{tr}}} \sum_{k,q} \sin(qa/2)^2 u_q (c_k^* c_{k-q} + C.C.). \quad (29)$$

The time evolution of the variables is defined by the Hamiltonian equations of motion

$$\frac{dc_k}{dt} = -\frac{i}{\hbar} \frac{\partial H}{\partial c_k^*}, \quad \frac{dc_k^*}{dt} = \frac{i}{\hbar} \frac{\partial H}{\partial c_k}, \quad \frac{du_k}{dt} = -\frac{\partial H}{\partial p_{-k}}, \quad \frac{dp_k}{dt} = \frac{\partial H}{\partial u_k}. \quad (30)$$

It is straightforward to check that these equations conserve both the total energy H and the optical phonon wavefunction normalization $\sum_q |c_k|^2 = 1$. This approximation treats classically all participating phonons.

A semiclassical approach is justified for optical phonons if anharmonic interactions are weak compared to harmonic ones

$$V_3 \ll \Delta_{\text{opt}}, \Delta_{\text{tr}}. \quad (31)$$

In this regime one can think of an optical phonon as a plane wave with a certain wavevector k undergoing rare scattering events. This justifies averaging of the nonlinear interactions over the optical phonon wavefunction implied in the classical equations Eq. (30). The semiclassical approach can miss the effect of quantum discreteness [41], though the analysis of the minimalist system of weakly anharmonically coupled oscillators shows similarity between classical and quantum considerations [44].

Below we focus on modelling the relaxation in the regimes of the smallest numbers of sites N , where Fermi's golden rule in the form of Eq. (19) ($N = 20$ and $r < 1$) or Eq. (21) ($N = 48$ and $r > 1$) is still applicable for a reasonable anharmonic coupling strength $V_3 \geq 0.01\Delta_{\text{opt}}$. In both cases we choose the initial midband optical phonon state with the wavevector $k = 2\pi n/L$ and $n = N/4$ with one exception related to the investigation of the dependence of the relaxation rate on the initial state. The dynamics for smaller numbers of sites is slower and contains oscillations determined by rare resonances similarly to Ref. [45]. Its consideration is beyond the scope of the present work.

In our calculations we set the thermal energy equal to the double bandwidth for transverse acoustic phonons $k_B T = 2\hbar\Delta_{\text{tr}}$. At that temperature the classical approximation is reasonably justified, while the temperature under consideration is not much higher than the room temperature where $k_B T \sim \hbar\Delta_{\text{tr}}$. Consequently, our results are valid at room temperature at least qualitatively.

2. Results of calculations

At time $t = 0$ the optical phonon is placed to the state with a certain wavevector k similarly to Sec. IV A. For transverse acoustic phonons we choose zero initial coordinates $u_q = 0$ and random momenta $p_q = p_{-q} = \xi_q \sqrt{2Mk_B T}$, where ξ_q are random numbers generated from the Gaussian distribution with a unit width. These initial conditions introduce the relevant temperature if anharmonic interaction is weak Eq. (30) so kinetic and potential energies for each normal mode should be approximately equal to $k_B T/2$.

Time dependencies of probabilities $P_k(t) = |c_k(t)|^2$ are calculated solving the Hamiltonian equations Eq. (30) and averaging their solutions over many random initial conditions corresponding to the given temperature until the accuracy of few percents is obtained. Below the results of calculations are reported for time dependent probabilities P_k for different system sizes, anharmonic coupling strengths and bandwidth ratios r .

First, we report time dependent currents for representative chain of $N = 20$ sites with initially excited midband optical phonon. The anharmonic coupling was chosen as $V_3 = 0.05\sqrt{\Delta_{\text{opt}}\Delta_{\text{tr}}}$ to have bandwidth independent Fermi's golden rule rates of emission and absorption Eq. (19). The absolute value of V_3 and the system size were chosen to avoid discreteness and have perturbation theory applicable. Remember that the temperature is given by $k_B T = 2\hbar\Delta_{\text{tr}}$.

Time dependencies of current are very different for $r \leq 1$ where it can be characterized by a single relaxation time and $r \geq 2$ where it relaxes in two stages including the fast initial relaxation during the time of the order of one picosecond and a slow subsequent relaxation taking orders of magnitude longer. This observation is consistent with the expectations of Sec. III A 2. For $N = 20$ and $r > 1$ there are some discreteness effects that are seen in Fig. 5 as damped oscillations emerging due to three or four phonon resonances. We do not consider them in detail.

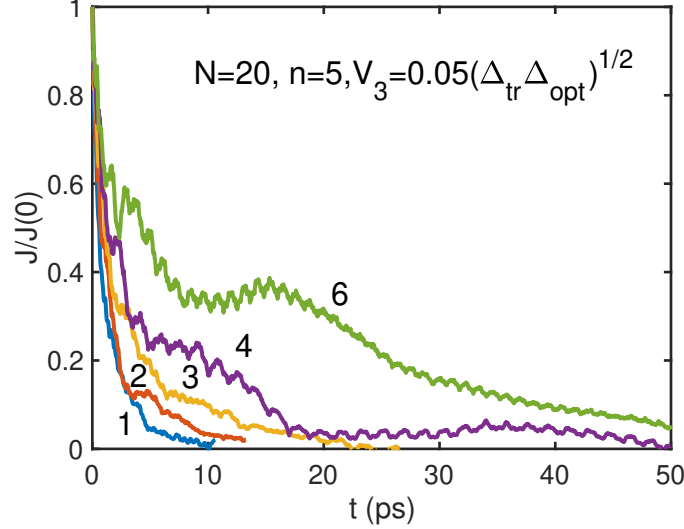


FIG. 5: Time dependence of current for different ratios (r) of acoustic to optical bandwidth indicated near each graph.

To characterize both regimes we examine relaxation time behaviors separately in Sec. IV B 3 for a small bandwidth ratio $r = 1/2$ and in Sec. IV B 4 in the opposite regime of $r > 1$.

3. Relaxation at small bandwidth ratio ($r = 1/2$)

For $r \leq 1$ it is natural to expect a population relaxation following the Fermi's golden rule predictions at high temperature Eq. (19). To verify that, we examined the population relaxation for the bandwidth ratio $r = 1/2$ and all possible initial wavevectors k for $N = 20$ as reported in Fig. 6. The relaxation time for each initial state time dependent population $P_n(t)$ corresponding to the wavevector $k = 2\pi n/L$ was estimated setting $P_n(T_{\text{rel}}(n)) = P_n(\infty) + (1 - P_n(\infty))e^{-1}$, where $P_n(\infty) \approx 1/N$ is the infinite time limit of the phonon state population in the classical ergodic system. Exact time averaged populations slightly differ from each other for different wavevectors, but this difference is negligible for the temperature under consideration due to the conservation of the number of optical phonons and their classical treatment.

To compare the numerical results for relaxation times with the theory Eq. (19) predicting that

$$T_{\text{rel}}(n) = \frac{\hbar\Delta_{\text{tr}}\Delta_{\text{opt}} \sin(|n|\pi/N)}{16V_3^2 k_B T}$$

we plot the ratios $T_{\text{rel}}(n)/\sin(n\pi/N)$ vs n which should be independent of the initial wavevector in Fig. 6.a. Only half of initial wavevectors is shown since the data for n and $-n$ are identical due to the inversion symmetry. We did not examine lifetimes of the states with $n = 0$ and $N/2$ where the Fermi's golden rule must obviously fail.

According to our observations the results for the relaxation rate are in an excellent agreement with the theory for $N = 20$ and $2 \leq n \leq 8$. The deviations at small wavevectors are probably because the predicted relaxation rate is too fast there, so the Fermi's golden rule is no longer applicable (see discussion in Sec. III C 1). The dependence of the relaxation time on the anharmonic interaction $T_{\text{rel}} \propto V_3^{-2}$ is also consistent with the theory predictions except for very small coupling constants $V_3 \leq 0.01\Delta_{\text{opt}}$ where discreteness becomes significant as shown in Fig. 6.b.

4. Relaxation at large bandwidth ratio $r > 1$

For a large bandwidth ratio $r \geq 2$ the evolution of current cannot be described using a single relaxation time as it is clearly seen in Fig. 5. The current relaxes in two stages including the first fast stage taking few picoseconds due to absorption or emission Eq. (19) (forward scattering) and the second slow stage that is expected to be determined by much slower phonon scattering Eq. (21) (backscattering). Here we report the results for the slow stage relaxation

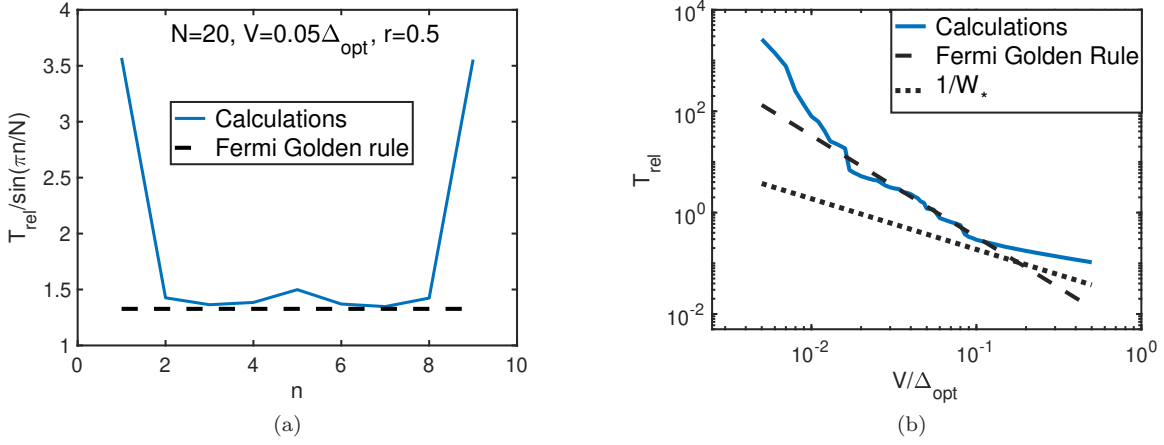


FIG. 6: (a) Dependence of the rescaled relaxation time on the wavevector for $N = 20$ compared to the Fermi's golden rule result Eq. (19) for the parameters $k_B T = 2\Delta_{\text{tr}}$, $V = 0.05\Delta_{\text{opt}}$, $r = 0.5$. (b) Dependence of the relaxation time on the strength of the anharmonic interaction for the same parameters as in (a) and $n = 5$. Results are compared with the Fermi's golden rule Eq. (19) (dashed line) and the minimum relaxation time $1/W_*$ Eq. (24) (dotted line).

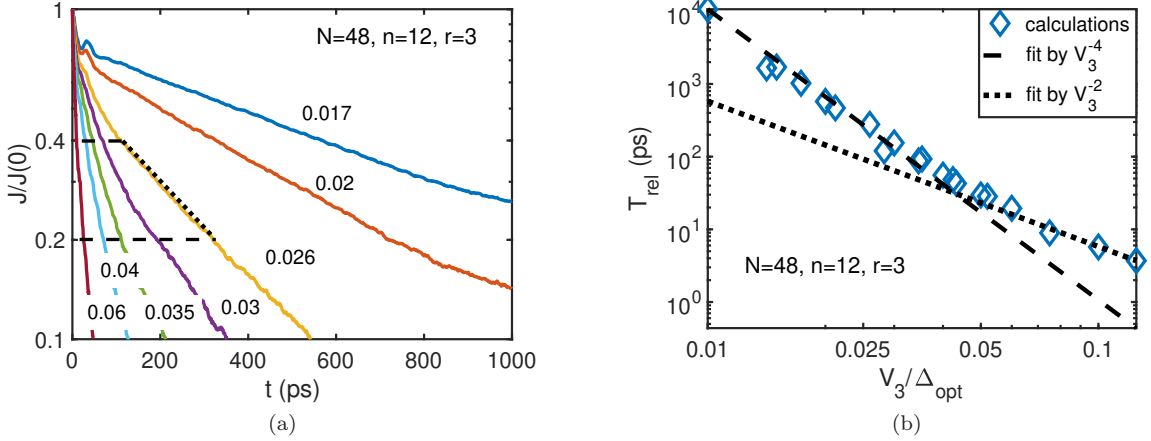


FIG. 7: (a) Time dependence of current for initially excited midband optical phonon and different anharmonic coupling strengths V_3/Δ_{opt} shown near each curve. The negative inverse slope of the dashed line serves as an estimate for the relaxation time. (b) Dependence of relaxation times on anharmonic coupling strengths fitted by V_3^{-4} dependence for small couplings (dashed line) and V_3^{-2} dependence for large couplings (dotted line). In both graphs the bandwidth ratio is $r = 3$.

for $N = 48$ and compare the current evolution at the slow stage with the predictions of theory Eq. (21). We always excite initially the midband optical phonon $n = 12$ and use the temperature corresponding to the thermal energy exceeding the transverse phonon bandwidth twice $k_B T = 2\hbar\Delta_{\text{tr}}$.

First we report the results for the representative bandwidth ratio $r = 3$ in Fig. 7. In Fig. 7.a the time evolution of currents is shown for different anharmonic coupling constants. The current clearly relaxes in two stages and we focus on the second stage. To extract the relaxation time we fit the current time dependence by a single exponent for the part of relaxation occurring between $J/J(0) = 0.4$ and $J/J(0) = 0.2$ as shown by the dashed line. The relaxation time is estimated using the negative inverse slope of this line. The results are sensitive to the fitting domain (use of the specific points $J/J(0) = 0.4$ and 0.2 to extract the relaxation rate), since relaxation is getting slower with time possibly reflecting its diffusive nature. Our estimate gives a right guess about the time of the transition between ballistic and diffusive regimes. and parametric dependencies of this time nearly insensitive to its specific definition.

The relaxation time dependence on the anharmonic coupling strength is shown in Fig. 7. At relatively small coupling $V_3 \leq 0.05\Delta_{\text{opt}}$ this dependence is perfectly consistent with the theory prediction of the inverse fourth power dependence Eq. (21), while at large V it switches to the weaker dependence probably because of the failure of the

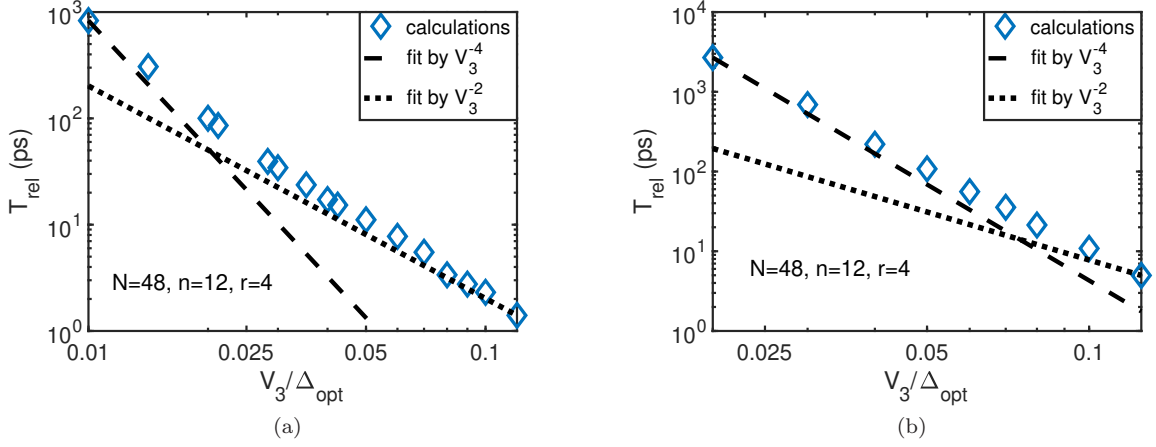


FIG. 8: Dependence of relaxation times on anharmonic coupling strengths for $r = 2$ (a) and $r = 4$ (b) fitted similarly to Fig. 7.

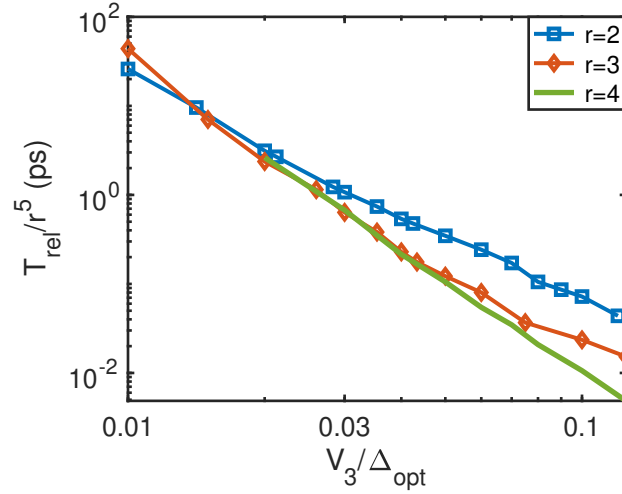


FIG. 9: Dependence of rescaled relaxation times on anharmonic coupling for different bandwidth ratios.

Fermi's golden rule as a perturbation theory.

Similar scaling of relaxation times is obtained for other two considered bandwidth ratios $r = 2$ and $r = 4$ as illustrated in Fig. 8.a and b, respectively. The dependence V_3^{-4} is seen in a wider domain for $r = 4$ and in a very narrow domain for $r = 2$ compared to $r = 3$ that is the consequence of different separations from the threshold at $r = 1$.

We also examine the dependence of relaxation times on the bandwidth ratio. In our regime of interest $k_B T = 2\hbar\Delta_{\text{tr}}$ the expected dependence can be expressed following Eq. (21) as $T_{\text{rel}} = r^5 \Delta_{\text{opt}}^3 / (4CV_3^4)$. To check the relevance of this dependence we plot the rescaled relaxation times T_{rel}/r^5 in Fig. 9 for $r = 2, 3$ and 4 . The graphs for the bandwidth ratios $r = 3$ and 4 are perfectly consistent with the theory expectations. The dependence for $r = 2$ deviates from those expectations. This deviation is possibly because the case $r = 2$ is close to the crossover regime $r = 1$. Two approaches are getting consistent for $r = 2$ at small V_3 if we use the resonant coupling r dependence $V(k, -k, -k, k) \propto 1/(r^2 - 1)$ (see Eq. (26)) to estimate the effective scattering matrix element replacing expected r^5 relaxation time dependence with $r(r^2 - 1)^2$.

Using the numerical estimate of the relaxation time we can find the dimensionless constant C in Eq. (21) as $2.7 \cdot 10^4$. This dimensionless numerical factor is huge, but this is not so surprising. The typical transition matrix element $V(k, -k, -k, k)$ Eq. (26) contains a large numerical factor of $\eta_4 = 16$. At high temperature it also acquires a factor expressing the number of thermal phonons $k_B T / (\hbar\omega_{\text{tr}}(k))$ estimated in Eq. (21) as $k_B T / (\hbar\Delta_{\text{tr}})$. However, the actual energy $\hbar\omega_{\text{tr}}(k)$ for the initial midband state $k = \pi/(2a)$ is a half of the bandwidth, so an extra factor of two

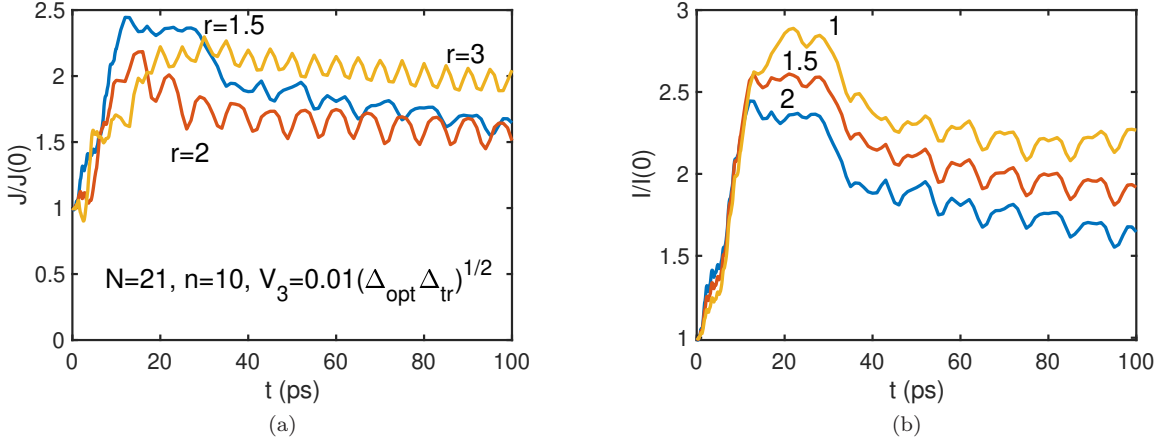


FIG. 10: (a) Raise of current due to anharmonic interaction for the initial state with a small group velocity ($N = 21$, $n = 10$) and different bandwidth ratios r shown for each graph. The temperature is fixed at $k_B T = 2\hbar\Delta_{tr}$. (b) Current for the bandwidth ratio $r = 1.5$ at different temperatures. The ratio $k_B T / (\hbar\Delta_{tr})$ is shown above each graph.

naturally appears in the definition of the matrix element modifying the numerical factor to $2\eta_4 \sim 32$. The squared matrix element within the Fermi's golden rule acquires this numerical factor squared that is $32^2 \approx 1000$.

The remaining factor of $C/32^2 \approx 27$ in the definition of the current relaxation rate can be originated from the integration over two wavevectors in the related Fermi's-golden rule expression for the current relaxation rate (see Refs. [46, 47]). Another possible origin for the extra rate enhancement factor of order of 10 can be due to a multistep current evolution involving first fast relaxation of the phonon to one of the states with a smaller energy with a subsequent backscattering from that state that can happen faster compared to that from the initial state due to larger number of participating transverse phonons at lower energies. Thus, the large numerical factor C is quite reasonable for the current relaxation rate.

V. ACCELERATION OF TRANSPORT FOR A SMALL INITIAL VELOCITY OF OPTICAL PHONON

We demonstrated in Secs. III, IV that the evolution of an optical phonon due to its interaction with transverse phonons for the bandwidth ratio (transverse to optical ones) greater than unity can be separated into two stages. In the first, fast stage the phonon is scattered only forward, so its average velocity remains finite as for the ballistic transport. Consequently, in the first stage we observed numerically the fast current reduction to some finite value Fig. 5. This reduction is because the initial midband state used in Sec. IV possesses the maximum velocity. If the initial state is chosen near band edges, where the velocity approaches minimum, then the forward scattering to other faster states should increase the velocity. This is an interesting and untypical regime, where the relaxation enhances the current.

Such acceleration can possibly explain the recently discovered increase of the optical phonon ballistic transport velocity in alkane chains with the chain length [29]. The measurements carried out similarly to the earlier work [23] show that the phonon velocity increases with increasing the chain length from $14\text{\AA}/\text{ps}$ for shorter chains to around $48\text{\AA}/\text{ps}$ for longer chains containing more than 20 CH_2 groups. If the propagating wavepacket is initiated at the top of a band where the group velocity is small, it can be scattered towards the midband states, featuring much larger group velocities, still propagating in the forward direction. Since such a process became efficient at longer chains where the phonon has sufficient time for scattering, it would result in a speed increase. Several optical bands of alkane chains can fit such conditions, including CH_2 wagging, CH_2 rocking, and C–C stretching bands [48]. Then, in long chains the phonon gets re-scattered forward to midband states possessing much bigger group velocities up to $60\text{\AA}/\text{ps}$. This redistribution emerges during the first stage of relaxation taking few picoseconds, while the second stage taking time orders of magnitude longer is possibly not reached yet.

To demonstrate the optical phonon acceleration numerically we tried a variety of model parameters always choosing the initially excited optical phonon with a smallest (yet nonzero) velocity for different numbers of sites N and anharmonic coupling strengths V_3 . The high temperature semiclassical regime ($k_B T = 2\hbar\Delta_{tr}$) is considered since we observed a substantial increase of current only for $N > 20$ sites, where an accurate quantum mechanical treatment is problematic. Below we report a substantial increase of current for $N = 21$ with the initial state wavevector $k = 2\pi n/L$

and $n = 10$ possessing the minimum group velocity.

For our study we choose an anharmonic coupling strengths $V_3 = 0.01\sqrt{\Delta_{\text{opt}}\Delta_{\text{tr}}}$ for bandwidth ratios 1.5, 2, 3 similarly to Sec. III B 1. The absolute value of V_3 was chosen using guess and check method to maximize the current rise. The time dependence of current for these specific parameters is shown in Fig. 10.a.

According to Fig. 10.a, the current rises in the fast stage taking around 10 ps by factor of 2 or even 2.5 depending on the specific bandwidth ratio. The slow stage takes orders of magnitude longer, yet it limits the maximum current raise. The strongest increase of current is observed for a smallest considered bandwidth ratio of $r = 1.5$.

The verification of the proposed interpretation of the experimental data can be made modifying the temperature, which is the only controlling parameter that can be changed relatively easily and can be modeled using the present theory. The effect of temperature is reported in Fig. 10.B. The rise of the current and, correspondingly, maximum transport velocity is clearly seen with the reduction of the temperature and it can be probed experimentally to validate the present theory. This rise with decreasing the temperature could be due to the suppression of slow backscattering processes limiting the raise of the current. One should notice, however, that further reduction in temperature can reduce the transport rate due to phonon redistribution towards lower energies corresponding to their Boltzmann distribution.

VI. CONCLUSIONS

We examined transport and decoherence of optical phonons in periodic chains due to their interaction with transverse acoustic phonons. Similarly to the earlier work [18], where the interaction with longitudinal acoustic phonons was considered, we found two distinguishable dynamic regimes depending on the relationship between acoustic and optical phonon bandwidths.

In the typical regime of a narrower optical phonon band compared to acoustic phonon bands an optical phonon relaxation within the band emerges in two stages. The first stage takes several picoseconds. It includes fast equilibration of the initially excited optical phonon within the band states featuring similarly directed group velocities by means of forward scattering accompanied by absorption or emission of transverse acoustic phonons forbidden for longitudinal phonons due to the Cherenkov’s constraint [18]. Importantly, this forward only scattering supports the ballistic transport.

If the initial optical phonon velocity is smaller than its average velocity, then the phonon accelerates due to forward scattering to the states with a higher velocity. The latter regime is possibly realized in the recent measurements of energy transport through alkane chains, where the optical phonon velocity increases with increasing the chain length [29].

The second stage of phonon relaxation involves its backscattering. It converts the ballistic transport regime to diffusive but takes much longer time. The backscattering occurs much slower compared to the forward scattering in the first stage, because for narrow optical bands it requires higher order anharmonic interactions.

If the acoustic band is narrower (bandwidth ratio r less than unity) then the optical phonon relaxes very quickly in about a few picoseconds from its initial state to all other states within the band. This relaxation leads to the substantial current reduction and changing the transport from ballistic to diffusive.

Usually, acoustic phonon bands are wider compared to optical phonon bands [18, 23]. However, our results for the opposite regime are also relevant for other systems of interest including, for example, electrons propagating in periodic molecules. The electron energy band can be broader than any phonon band, so the situation of $r < 1$ is quite realistic.

ACKNOWLEDGMENTS

This work was supported by the National Science Foundation (Grant No. CHE-2201027).

* aburin@tulane.edu

¹ A. Nitzan, “Molecules take the heat,” *Science* **317**, 759–760 (2007).

² David M. Leitner, “Quantum ergodicity and energy flow in molecules,” *Advances in Physics* **64**, 445–517 (2015).

³ Hari Datt Pandey and David M. Leitner, “Thermalization and thermal transport in molecules,” *The Journal of Physical Chemistry Letters* **7**, 5062–5067 (2016).

⁴ David M. Leitner, Hari Datt Pandey, and Korey M. Reid, “Energy transport across interfaces in biomolecular systems,” *The Journal of Physical Chemistry B* **123**, 9507–9524 (2019).

- ⁵ Sourav Karmakar and Srihari Keshavamurthy, “Intramolecular vibrational energy redistribution and the quantum ergodicity transition: a phase space perspective,” *Phys. Chem. Chem. Phys.* **22**, 11139–11173 (2020).
- ⁶ Jan Paulo T. Zaragoza, Adam R. Offenbacher, Shenshen Hu, Christine L. Gee, Zachary M. Firestein, Natalie Minnetian, Zhenyu Deng, Flora Fan, Anthony T. Iavarone, and Judith P. Klinman, “Temporal and spatial resolution of distal protein motions that activate hydrogen tunneling in soybean lipoxygenase,” *Proceedings of the National Academy of Sciences* **120**, e2211630120 (2023), <https://www.pnas.org/doi/pdf/10.1073/pnas.2211630120>.
- ⁷ Yifeng Jiang, Lai Chung Liu, Antoine Sarracini, Kamil M. Krawczyk, Jordan S. Wentzell, Cheng Lu, Ryan L. Field, Samir F. Matar, Wojciech Gawelda, Henrike M. Müller-Werkmeister, and R. J. Dwayne Miller, “Direct observation of nuclear reorganization driven by ultrafast spin transitions,” *Nature Communications* **11**, 1530 (2020).
- ⁸ Taishan Zhu, Krishnan Swaminathan-Gopalan, Kevin J. Cruse, Kelly Stephani, and Elif Ertekin, “Vibrational energy transport in hybrid ordered/disordered nanocomposites: Hybridization and avoided crossings of localized and delocalized modes,” *Advanced Functional Materials* **28**, 1706268 (2018), <https://onlinelibrary.wiley.com/doi/pdf/10.1002/adfm.201706268>.
- ⁹ D. Segal, A. Nitzan, and P. Hänggi, “Thermal conductance through molecular wires,” *J. Chem. Phys.* **119**, 6840–6855 (2003).
- ¹⁰ Zhaohui Wang, Jeffrey A. Carter, Alexei Lagutchev, Yee Kan Koh, Nak-Hyun Seong, David G. Cahill, and Dana D. Dlott, “Ultrafast flash thermal conductance of molecular chains,” *Science* **317**, 787–790 (2007), <http://science.sciencemag.org/content/317/5839/787.full.pdf>.
- ¹¹ Asegun Henry and Gang Chen, “High thermal conductivity of single polyethylene chains using molecular dynamics simulations,” *Phys. Rev. Lett.* **101**, 235502 (2008).
- ¹² Dvira Segal and Bijay Kumar Agarwalla, “Vibrational heat transport in molecular junctions,” *Annual Review of Physical Chemistry* **67**, 185–209 (2016), PMID: 27215814, <https://doi.org/10.1146/annurev-physchem-040215-112103>.
- ¹³ Dvira Segal, Abraham Nitzan, and Peter Hänggi, “Thermal conductance through molecular wires,” *The Journal of Chemical Physics* **119**, 6840–6855 (2003), <https://doi.org/10.1063/1.1603211>.
- ¹⁴ Renai Chen, Inon Sharony, and Abraham Nitzan, “Local atomic heat currents and classical interference in single-molecule heat conduction,” *The Journal of Physical Chemistry Letters* **11**, 4261–4268 (2020).
- ¹⁵ Bernd Gotsmann, Andrea Gemma, and Dvira Segal, “Quantum phonon transport through channels and molecules? A Perspective,” *Applied Physics Letters* **120**, 160503 (2022), https://pubs.aip.org/aip/apl/article-pdf/doi/10.1063/5.0088460/16446345/160503_1_online.pdf.
- ¹⁶ Igor V. Rubtsov and Alexander L. Burin, “Ballistic and diffusive vibrational energy transport in molecules,” *The Journal of Chemical Physics* **150**, 020901 (2019), <https://doi.org/10.1063/1.5055670>.
- ¹⁷ Longji Cui, Sunghoon Hur, Zico Alaia Akbar, Jan C. Klöckner, Wonho Jeong, Fabian Pauly, Sung-Yeon Jang, Pramod Reddy, and Edgar Meyhofer, “Thermal conductance of single-molecule junctions,” *Nature* (2019), 10.1038/s41586-019-1420-z.
- ¹⁸ Alexander L. Burin, Igor V. Parshin, and Igor V. Rubtsov, “Maximum propagation speed and Cherenkov effect in optical phonon transport through periodic molecular chains,” *The Journal of Chemical Physics* **159**, 054903 (2023), https://pubs.aip.org/aip/jcp/article-pdf/doi/10.1063/5.0158201/18069436/054903_1_5.0158201.pdf.
- ¹⁹ I. V. Rubtsov, “Relaxation-assisted two-dimensional infrared (ra 2d ir) method: Accessing distances over 10 angstrom and measuring bond connectivity patterns,” *Acc. Chem. Res.* **42**, 1385–1394 (2009).
- ²⁰ Natalia I. Rubtsova, Layla N. Qasim, Arkady A. Kurnosov, Alexander L. Burin, and Igor V. Rubtsov, “Ballistic energy transport in oligomers,” *Accounts of Chemical Research* **48**, 2547–2555 (2015), PMID: 26305731.
- ²¹ Tammy X. Leong, Layla N. Qasim, Robert T. Mackin, Yuchen Du, Robert A. Pascal, and Igor V. Rubtsov, “Unidirectional coherent energy transport via conjugated oligo(p-phenylene) chains,” *The Journal of Chemical Physics* **154**, 134304 (2021), <https://doi.org/10.1063/5.0046932>.
- ²² Igor V. Rubtsov, “Relaxation-assisted two-dimensional infrared (ra 2dir) method: Accessing distances over 10 Å and measuring bond connectivity patterns,” *Accounts of Chemical Research* **42**, 1385–1394 (2009).
- ²³ Natalia I. Rubtsova, Clara M. Nyby, Hong Zhang, Boyu Zhang, Xiao Zhou, Janarthanan Jayawickramarajah, Alexander L. Burin, and Igor V. Rubtsov, “Room-temperature ballistic energy transport in molecules with repeating units,” *The Journal of Chemical Physics* **142**, 212412 (2015), <https://doi.org/10.1063/1.4916326>.
- ²⁴ Layla N. Qasim, E. Berk Atuk, Andrii O. Maksymov, Janarthanan Jayawickramarajah, Alexander L. Burin, and Igor V. Rubtsov, “Ballistic transport of vibrational energy through an amide group bridging alkyl chains,” *The Journal of Physical Chemistry C* **123**, 3381–3392 (2019).
- ²⁵ Arkady A. Kurnosov, Igor V. Rubtsov, and Alexander L. Burin, “Communication: Fast transport and relaxation of vibrational energy in polymer chains,” *The Journal of Chemical Physics* **142**, 011101 (2015), <http://dx.doi.org/10.1063/1.4905076>.
- ²⁶ Natalia I. Rubtsova, Arkady A. Kurnosov, Alexander L. Burin, and Igor V. Rubtsov, “Temperature dependence of the ballistic energy transport in perfluoroalkanes,” *The Journal of Physical Chemistry B* **118**, 8381–8387 (2014), PMID: 24697782.
- ²⁷ Layla N. Qasim, Arkady Kurnosov, Yuankai Yue, Zhiwei Lin, Alexander L. Burin, and Igor V. Rubtsov, “Energy transport in peg oligomers: Contributions of different optical bands,” *The Journal of Physical Chemistry C* **120**, 26663–26677 (2016).
- ²⁸ Alexei Boulatov and Alexander L. Burin, “Crucial effect of transverse vibrations on the transport through polymer chains,” *The Journal of Chemical Physics* **153**, 134102 (2020), <https://doi.org/10.1063/5.0018591>.
- ²⁹ Sithara U. Nawagamuwage, Elliot S. Williams, Md Muhaiminul Islam, Igor V. Parshin, Alexander L. Burin, Nathalie Busschaert, and Igor V. Rubtsov, “Ballistic energy transport via long alkyl chains: A new initiation mechanism,” (2024), arXiv:2405.13776 [physics.chem-ph].

- ³⁰ Alexander Burin, Andrii Maksymov, Ma?ayan Schmidt, and Il?ya Polishchuk, “Chaotic dynamics in a quantum fermi-pasta-ulam problem,” *Entropy* **21**, 51 (2019).
- ³¹ Kittusamy Senthilkumar, Ferdinand C. Grozema, Célia Fonseca Guerra, F. Matthias Bickelhaupt, Frederick D. Lewis, Yuri A. Berlin, Mark A. Ratner, and Laurens D. A. Siebbeles, “Absolute rates of hole transfer in dna,” *Journal of the American Chemical Society* **127**, 14894–14903 (2005).
- ³² Yuankai Yue, Layla N. Qasim, Arkady A. Kurnosov, Natalia I. Rubtsova, Robert T. Mackin, Hong Zhang, Boyu Zhang, Xiao Zhou, Janarthanan Jayawickramarajah, Alexander L. Burin, and Igor V. Rubtsov, “Band-selective ballistic energy transport in alkane oligomers: Toward controlling the transport speed,” *The Journal of Physical Chemistry B* **119**, 6448–6456 (2015), PMID: 25936983.
- ³³ L.D. Landau, E.M. Lifšic, E.M. Lifshitz, A.M. Kosevich, J.B. Sykes, L.P. Pitaevskii, and W.H. Reid, *Theory of Elasticity: Volume 7*, Course of theoretical physics (Elsevier Science, 1986).
- ³⁴ Gnther Hartwig, *Polymer Properties at Room and Cryogenic Temperatures* (Springer, Boston, MA, 1994) pp. 17–46.
- ³⁵ L. Chico, R. Pérez-Álvarez, and C. Cabrillo, “Low-frequency phonons in carbon nanotubes: A continuum approach,” *Phys. Rev. B* **73**, 075425 (2006).
- ³⁶ Ronald F. Gibson, Emmanuel O. Ayorinde, and Yuan-Feng Wen, “Vibrations of carbon nanotubes and their composites: A review,” *Composites Science and Technology* **67**, 1 – 28 (2007).
- ³⁷ Charles Kittel, *Introduction to Solid State Physics*, 8th ed. (Wiley, 2004).
- ³⁸ Raffaele Borrelli and Maxim F Gelin, “Quantum dynamics of vibrational energy flow in oscillator chains driven by anharmonic interactions,” *New Journal of Physics* **22**, 123002 (2020).
- ³⁹ J. R. Schrieffer and P. A. Wolff, “Relation between the anderson and kondo hamiltonians,” *Phys. Rev.* **149**, 491–492 (1966).
- ⁴⁰ David M. Leitner, “Vibrational energy transfer in helices,” *Phys. Rev. Lett.* **87**, 188102 (2001).
- ⁴¹ David M. Leitner and Peter G. Wolynes, “Quantization of the stochastic pump model of arnold diffusion,” *Phys. Rev. Lett.* **79**, 55–58 (1997).
- ⁴² David E. Logan and Peter G. Wolynes, “Quantum localization and energy flow in manydimensional fermi resonant systems,” *The Journal of Chemical Physics* **93**, 4994–5012 (1990).
- ⁴³ V.L. Berezinskii and L.P. Gor’kov, “On the theory of electrons localized in the field of defects,” *Zh. Eksp. Teor. Fiz.* **77**, 2498 (1979), [*Sov. Phys. - JETP* **50**, 1209 (1979)].
- ⁴⁴ Igor Tikhonenkov, Amichay Vardi, James R. Anglin, and Doron Cohen, “Minimal fokker-planck theory for the thermalization of mesoscopic subsystems,” *Phys. Rev. Lett.* **110**, 050401 (2013).
- ⁴⁵ Miguel Onorato, Lara Vozella, Davide Proment, and Yuri V. Lvov, “Route to thermalization in the fermi–pasta–ulam system,” *Proceedings of the National Academy of Sciences* **112**, 4208–4213 (2015), <http://www.pnas.org/content/112/14/4208.full.pdf>.
- ⁴⁶ L.P. Pitaevskii and E.M. Lifshitz, *Physical Kinetics: Volume 10*, v. 10 (Elsevier Science, 2012).
- ⁴⁷ K. Busch, C. M. Soukoulis, and E. N. Economou, “Transport and scattering mean free paths of classical waves,” *Phys. Rev. B* **50**, 93–98 (1994).
- ⁴⁸ Sithara U. Nawagamuwage, Layla N. Qasim, Xiao Zhou, Tammy X. Leong, Igor V. Parshin, Janarthanan Jayawickramarajah, Alexander L. Burin, and Igor V. Rubtsov, “Competition of several energy-transport initiation mechanisms defines the ballistic transport speed,” *The Journal of Physical Chemistry B* **125**, 7546–7555 (2021).

